Fluorescence Probes

DOI: 10.1002/anie.201403918

Water-Soluble Triarylboron Compound for ATP Imaging In Vivo Using Analyte-Induced Finite Aggregation**

Xiaoyan Li, Xudong Guo, Lixia Cao, Zhiqing Xun, Shuangqing Wang, Shayu Li, Yi Li,* and Guoqiang Yang**

Abstract: *Adenosine 5′-triphosphate (ATP) is a multifunctional molecule that participates in many important biological processes. Currently, fluorescence indicators for ATP with high performance are in demand. Reported herein is a novel water-soluble triarylboron compound which displays an apparent ATP-dependent fluorescence enhancement when dispersed in water. It can selectively recognize ATP from other bioactive substances in vitro and in vivo. The ATP-induced finite aggregation endows the indicator with appreciable photostability and superior tolerance to environmental electrolytes. This indicator has been successfully applied to the ATP imaging in NIH/3T3 fibroblast cells. The difference in the ATP levels within the membrane and cytosol is clearly visible.*

Adenosine 5′-triphosphate (ATP), one of the best known biological compounds, is a multifunctional molecule found in all living organisms. As the major energy molecule of cells, ATP serves in a number of endothermic processes, including biosynthesis, active transport, cell division, muscle contraction, etc.[1] ATP is also critical in signal transduction processes. It is used as an intracellular precursor in kinase activity for proteins or lipids to provide a phosphate group, as well as in adenylate cyclase to produce the second messenger molecule cyclic adenosine monophosphate (cAMP).[2] Extracellular ATP serves as an activity-dependent signal for purinoceptors in nerve-mediated responses.[3] Visualization of ATP levels in vitro and in vivo can offer valuable information for precise understanding of these biological processes.

Classic measurements of ATP are based on offline analysis methods, such as HPLC, capillary electrophoresis, and NMR spectroscopy, of cell extracts.[4] In recent years, chemiluminescent recognition by luciferase and other enzymes have been developed.[5] However, the chemiluminescence method has a few limitations. First, suitable pH level, sufficient substrate, luciferin, and oxygen are indispensable in the recognition procedure. Second, the consumption of the analyte ATP and longer detection time make real-time observation difficult in practice.

Fluorescence indicators with high sensitivity, good selectivity, short response time, and the advantage of direct observation, are a powerful tool for the identification of substances in biological systems.[6] Despite ATP's significance in essential cellular processes, there are fewer studies on the development of effective ATP indicators in comparison to those on bioactive ions (e.g., Zn^{2+}, Ca^{2+}), possibly because of the difficulty of the mission. To date, biomolecule-based ATP indicators, such as luminophore-decorated ATP-binding proteins, DNA templates, and aptamers, have been successively implemented in eukaryotic cells,[7] but the expensive and difficult purification process significantly limits their practical applications. Passable ATP detections have also been achieved through low-cost chemical indicators which employ hydrogen bonding, electrostatic interactions, or metal–oxygen coordination,[8] though the interference from water, electrolytes, or partially dephosphorylated production of ATP are inevitable in practice.

In addition to the limitations, photostability under continual irradiation is a common challenge for conventional fluorescence indicators.[9] A reliable indicator must be photostable during the detection period, but apparent photobleaching is frequently observed for organic fluorophores at low concentrations. This situation is even more serious when the illumination source is a laser beam. Unfortunately, the low-concentration dye and the laser source are the most common requirements for fluorescence live-cell imaging. In contrast to other photophysical properties, such as absorption energy, emission wavelength, and fluorescence efficiency, photostability is an intrinsic property which is hard to improve even through structural modifications. Although fluorophores show a substantially slower bleaching rate in a solid matrix or other environments protected by a rigid shell,[10] the interactions of an indicator with an analyte are also hindered.

As a result of reducing the influences from the surrounding environment, nanoaggregates formed by organic fluorophores generally possess higher photostability compared to that of monodisperse molecules with the same molecular structure.[11] And a few nanoaggregates have been applied in long-term cell tracking.[12] However, the fluorescence quenching induced by aggregation is unavoidable for most fluoro-

[*] X. Y. Li, X. D. Guo, L. X. Cao, Dr. S. Q. Wang, Dr. S. Y. Li, Prof. Dr. G. Q. Yang
Beijing National Laboratory for Molecular Sciences
Key Laboratory of Photochemistry, Institute of Chemistry
Chinese Academy of Sciences, Beijing 100190 (China)
E-mail: shayuli@iccas.ac.cn
gqyang@iccas.ac.cn
Z. Q. Xun, Prof. Dr. Y. Li
Key Laboratory of Photochemical Conversion and Optoelectronic Materials, Technical Institute of Physics and Chemistry
Chinese Academy of Sciences, Beijing 100190 (China)
E-mail: yili@mail.ipc.ac.cn

[**] We are grateful for funding from the National Basic Research Program (2013CB834505, 2013CB834703, 2011CBA00905, and 2009CB930802) and the National Natural Science Foundation of China (grant nos 21233011, 91123033, 21273252, 21205122, 21261160488 and 21072196).

Supporting information for this article is available on the WWW under http://dx.doi.org/10.1002/anie.201403918.

phores because of the well-known aggregation-caused quenching (ACQ), which is a short-range interchromophoric energy migration and transfer.[13] To tackle the problems fluorescence indicators, we propose herein, the novel approach of analyte-induced finite aggregation. In this approach, the indicator molecules are separated by non-chromophoric analytes, so aggregation indeed happens but the ACQ effect is avoided. Although this work is focused on a novel ATP indicator, the approach could be extended to other indicators with lipophilic luminogens.

A triarylboron luminogen dipyren-1-yl (2,4,6-triisopropylphenyl)borane (DPTB) was synthesized and functionalized with the di(1*H*-imidazol-1-yl)methane dication (IMI) and 1-ethoxy-2-(2-methoxyethoxy)ethane (EG) moieties (DPTB-IMI-EG). DPTB is a typical charge-transfer (CT) compound known for its intense luminescence.[14] DPTB-IMI-EG also shows lower fluorescence efficiency in polar media, just like other CT compounds. The IMI is the triphosphate-targeting functional group which can discriminate between tri-, di-, and monophosphate groups upon binding.[8b] And the nonionic EG moiety improves the water solubility of the whole molecule. Moreover, the electropositive IMI and the lipophilic DPTB facilitate the entrance of the indicator into cell. When DPTB-IMI-EG meets with ATP in an aqueous environment, the electrostatic interaction will result in the formation of charge-neutralization complexes which immediately aggregate because of hydrophobic interactions (Scheme 1). The aggregate is significantly lower in polarity than physiological buffer because of the extrusion of water and electrolytes. So the fluorescence of DPTB can be increased by the so-called positive solvatokinetic effect. Moreover, nonchromophoric ATP molecules are abundant in the aggregates, thus preventing the approach of the luminogens and avoiding the ACQ. The results provided in this work indicate that DPTB-IMI-EG possesses high selectivity for ATP, appreciable photostability, and superior tolerance to environmental electrolytes. And this indicator is also used to detect ATP in living systems.

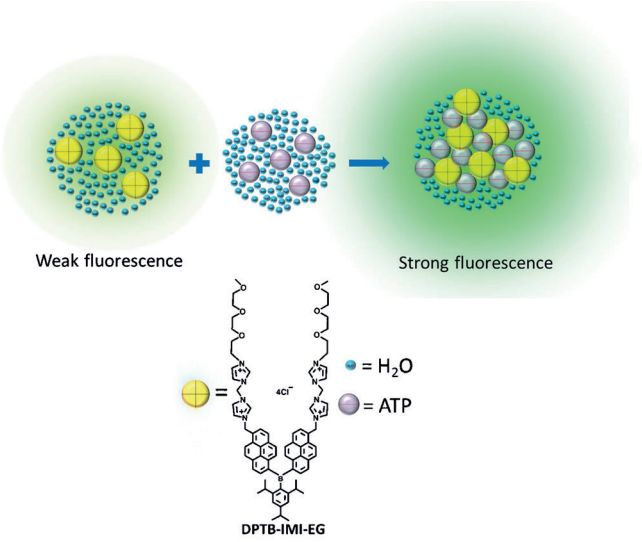

Scheme 1. The ATP indicator system.

Scheme S1 in the Supporting Information illustrates the synthetic route to DPTB-IMI-EG. The DPTB-CH_2Br moiety was first synthesized and subsequently reacted with the water-soluble IMI-EG moiety in DMF. The relatively long route is a compromise to separate the 6- and 8-substituted pyrene derivatives. Although DPTB is a large and lipophilic moiety, DPTB-IMI-EG is completely soluble in very strongly polar solvents such as DMSO, ethanol, and water, but is almost insoluble in acetone, acetonitrile, and ethyl acetate. This insolubility may be caused by the four positive charges of the molecule, and was utilized for the final purification process. DPTB-IMI-EG shows appreciable thermal stability with a decomposition temperature of over 220 °C.

Figures 1 a,b shows the absorption and fluorescence spectra of DPTB-IMI-EG with different amounts of ATP in vitro. The absorption band around $\lambda = 420$ nm decreases and shows a bathochromic shift, and an isosbestic point is observed at $\lambda = 430$ nm. A typical tail absorbance becomes

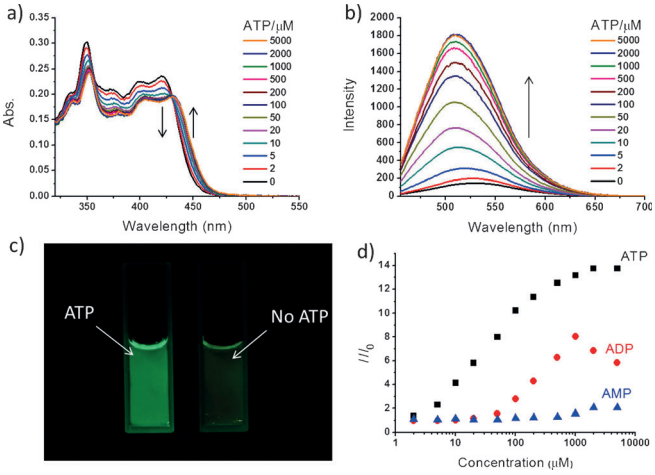

Figure 1. a) UV absorption and b) fluorescence spectral changes of DPTB-IMI-EG (10 μM) upon addition of the sodium salt of ATP (1–5000 μM). c) Photograph of DPTB-IMI-EG in the presence and absence of ATP (1 mM). d) Fluorescence titration curve of DPTB-IMI-EG upon the addition of AMP (blue), ADP (red), and ATP (black). I/I_0 means the fluorescence intensity ($\lambda = 510$ nm) changes and I_0 is the initial fluorescence intensity ($\lambda = 510$ nm) of DPTB-IMI-EG in the absence of nucleotides. Conditions: $\lambda_{ex} = 440$ nm, [DPTB-IMI-EG] = 10 μM, pH 7.4 (10 mM HEPES), 37 °C.

more obvious in the long-wavelength region, thus implying the formation of aggregates, which correlates well with dynamic light scattering (DLS) and scan electron microscopy (SEM) measurements (see Figure S2). The presence of ATP is more apparent through luminescence (Figure 1 c). Upon the addition of ATP, the maximum emission wavelength shows a slight hypsochromic shift and the fluorescence efficiency gradually increases (Table 1). It is crucial that the absorbance of the DPTB-IMI-EG/ATP composite is slightly longer than that of individual molecules, so that the fluorescence difference in the absence and presence of ATP can be amplified to over 12-fold when the excitation wavelength is $\lambda = 440$ nm. This amplification increases the detection contrast and improves the recognition sensitivity. The apparent dissocia-

Table 1: Quantum yield Φ of DPTB-IMI-EG at different ATP levels.

c [μM]	0	2	5	10	20	50
Φ	0.057	0.072	0.097	0.146	0.182	0.231
c [μM]	100	200	500	1000	2000	5000
Φ	0.293	0.311	0.334	0.359	0.383	0.378

tion constant (K_d) of the composite is determined as 51 μM by fitting plots of fluorescence intensity against ATP concentrations using the Hill equation. Thus, DPTB-IMI-EG can reliably detect ATP at levels higher than 0.1 mM.

As the partially dephosphorylated products of ATP, adenosine 5′-diphosphate (ADP) and adenosine 5′-monophosphate (AMP), are always present to some degree in any living cell, we further examined the specific characteristics of DPTB-IMI-EG selectivity for ATP over ADP and AMP in vitro. ADP results in qualitatively similar, but smaller changes in the spectra (Figure 1 d). For instance, the influence of 200 μM ADP on the fluorescence intensity is still smaller than that from ATP at 10 μM. The apparent dissociation constant (K_d) of DPTB-IMI-EG/ADP is determined as 460 μM by fitting the rising part of the ADP plot in Figure 1 d, and means that compared to ATP, DPTB-IMI-EG exhibits about a ninefold lower affinity for ADP. The fluorescence enhancements for an ATP solution and several ATP/ADP mixtures were also compared (see Figure S3), and taking into account the fact that ATP is five- to tenfold higher in concentration than ADP in living organisms,[15] we can conclude that ADP has no apparent influence on the test results when using the indicator DPTB-IMI-EG. The spectral changes with the addition of AMP are small enough to be ignored. The above results indicate that DPTB-IMI-EG as a fluorescence indicator has sufficient specificity for ATP under physiological conditions.

As ATP has several negatively charged groups under physiological conditions, it may chelate metals and other electrolytes with very high affinity.[16] The intracellular environment is complex, with large amounts of anions, cations, and many other charged biomolecules.[17] The interference from electrolytes is an ongoing design challenge for ATP indicators and little progress has been made in this respect. In our work, we recorded the fluorescence spectra of DPTB-IMI-EG with and without ATP in the presence of essential ions, amino acids, and proteins under physiological conditions. Three typical amino acids, Gly, Glu, and Lys, each with a different isoelectric point and two intracellular proteins, RNase A and chymotrypsinogen, were chosen as representative biomolecules and bio-macromolecules. As can be seen from Figure 2 a, only very slight fluorescence changes are observed when the indicator or indicator–ATP is exposed to these charged substances. This excellent tolerance for environmental electrolytes is in line with predictions. The neutral DPTB-IMI-EG/ATP consists of a large lipophilic section and a hydrophilic ether chain, and is similar to the structure of nonionic surfactants known for their negligible response to changes in ionic strength.[18] Additionally, the rather small K_d value of DPTB-IMI-EG/ATP is another crucial factor in the promising anti-interference performance.

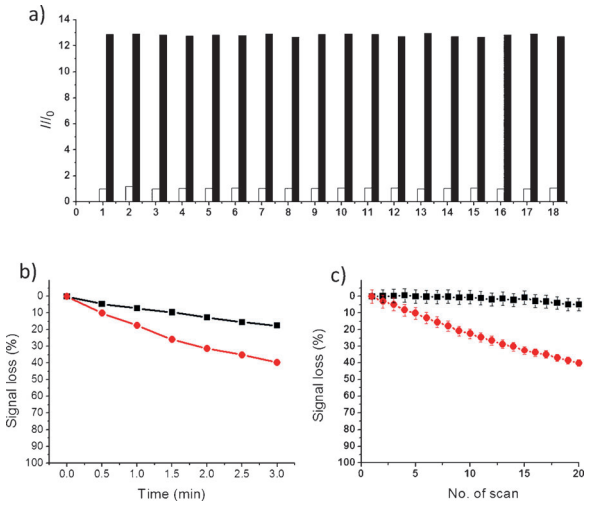

Figure 2. a) Fluorescence responses of DPTB-IMI-EG to various ions in the absence (white bars) and presence (black bars) of ATP (1 mM) at pH 7.4. 1) No ion, 2) Cl^- (5 mM), 3) I^- (1 mM), 4) NO_3^- (1 mM), 5) SO_4^{2-} (1 mM), 6) HCO_3^- (1 mM), 7) PPi (1 mM), 8) HPO_4^{2-} (1 mM), 9) AcO^- (1 mM), 10) Mg^{2+} (0.1 mM), 11) Fe^{2+} (0.1 mM), 12) Ca^{2+} (0.1 mM), 13) Zn^{2+} (0.1 mM), 14) Gly (1 mM), 15) Glu (1 mM), 16) Lys (1 mM), 17) RNase A (100 mg L^{-1}), 18) chymotrypsinogen (100 mg L^{-1}). b) Fluorescence intensity loss (%) of DPTB-IMI-EG (10 μM) in the presence (black) and absence (red) of ATP (1 mM) at pH 7.4 with increasing doses of UV ($\lambda = 365$ nm) exposure. c) Signal loss (%) of fluorescence emission of DPTB-IMI-EG (black) and MDRF (red) in vivo with an increasing number of scans. Excitation wavelength: $\lambda = 405$ nm (for DPTB-IMI-EG) and $\lambda = 635$ nm (for MDRF); emission wavelength: $\lambda = 460$–550 nm (for DPTB-IMI-EG) and $\lambda = 650$–730 nm (for MDRF); irradiation time: 10 s per scan.

Therefore we compared the photostability of DPTB-IMI-EG with and without ATP in vitro with the same $\lambda = 365$ nm excitation conditions. Although the fluorescence intensity of both systems decreases with increasing exposure, the experimental results clearly demonstrate that ATP considerably enhances the photostability of DPTB-IMI-EG (Figure 2 b). ATP presents an intensive absorption band at $\lambda = 260$ nm and no absorbance above $\lambda = 340$ nm, so the enhancement of photostability can only be derived from the aggregation of the luminophore. As revealed in Figure S2, DPTB-IMI-EG/ATP forms aggregates which show a monomodal size distribution with a hydrodynamic diameter of 297 nm in DLS measurements, and correlated well with SEM results. The aggregates can prevent interactions between the internal DPTB-IMI-EG and various external molecules, and significantly decreases the chance of photochemical reactions between the excited DPTB and active species such as water and oxygen. In contrast, the aggregation partially restricts the motion of DPTB, thus reducing the possibility of photoisomerization to some extent.[19] Thus, the aggregated luminophore possesses better photostability than the isolated molecule in solution.

For an indicator to be practically used in living organisms, its biocompatibility is the first and foremost criterion to be evaluated. The cytotoxicity of DPTB-IMI-EG on NIH/3T3 fibroblasts was examined by a standard 3-(4,5-dimethyl-2-thiazolyl)-2,5-diphenyltetrazolium bromide (MTT) assay. The indicator DPTB-IMI-EG has no obvious effects on the cell

viability, even at a high concentration of 4.0 μM (see Figure S4). Cell-membrane permeability is another important factor for evaluating the in vivo indicator because an indicator with poor permeability can only be used through harmful microinjection, electroporation, or scrape loading to load inside cells.[20] Fibroblast cells incubated with DPTB-IMI-EG for 30 minutes present strong fluorescence in the green channel, thus confirming the good permeability of the indicator (Figure 3 A1). DPTB-IMI-EG was then assessed for its photostability in vivo. A mitochondria dye, MitoTracker Deep Red FM (MDRF), was used as a reference material because of the lack of commercially available ATP imaging agent. The cells were co-stained with 1 μM DPTB-IMI-EG and 100 nM MDRF for 30 minutes, and excitation powers of two lasers ($\lambda = 405$ nm and $\lambda = 635$ nm) were unified as 100 μW. The fluorescence loss of DPTB-IMI-EG is less than 5% after 20 scans with total irradiation time of 200 seconds, thus demonstrating its greater photostability compared to that of MDRF (see Figure 2 c and Figure S5).

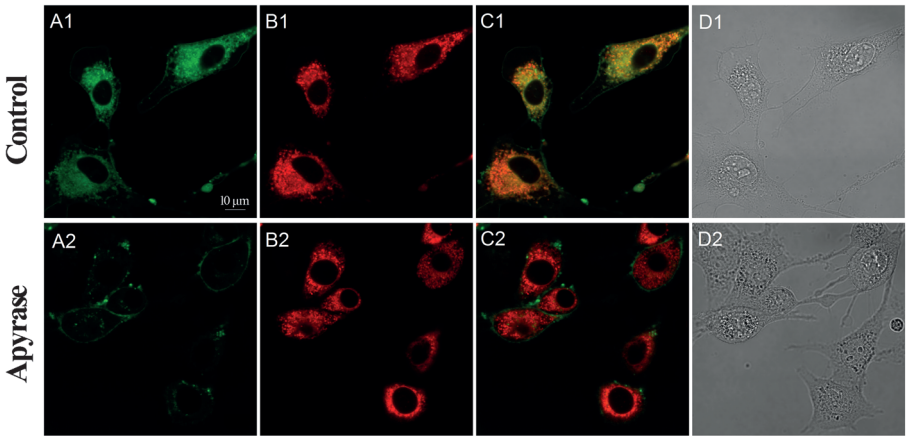

Figure 3. Confocal fluorescence images of live NIH/3T3 cells incubated with (A2–D2) or without (A1–D1) apyrase (1 U mL^{-1}) in DMEM for 60 min at 37 °C and then incubated with DPTB-IMI-EG and MDRF. A) Green channel for DPTB-IMI-EG (1 μM). B) Red channel for MDRF (100 nM). C) Panels A and B merged. D) Optical image.

The visualization of ATP distribution is essential for understanding its roles in vivo. DPTB-IMI-EG was investigated for its staining ability in living NIH/3T3 cells. The detailed fluorescence image presents apparent fluorescence signals only in the cytoplasm and cell membrane, but not in the nucleus (Figure 3 A1). The co-staining of DPTB-IMI-EG with MDRF illustrates that fluorescence regions of these two dyes seem to be highly overlapped in the cytoplasm (Figure 3 C1). The fluorescence signals of the MDRF and signals of the DPTB-IMI-EG in the cytoplasm are overlapped with $R_r = 0.86$. However, the two pieces of evidence demonstrate that the indicator is only close but not specific to the mitochondria in the cytoplasm. Firstly, the reticulum structures of the mitochondria are clearer in the image of MDRF-stained cell and secondly, the fluorescence intensity distributions of the two dyes are different in the pseudocolor images (see Figure S6). These images show that the ATP near the mitochondria is at a higher level than in other spaces within the cytoplasm. The uneven distribution of ATP is in line with expectations when we consider that the main source of ATP is generated by mitochondrial oxidative phosphorylation in eukaryotic cells.[21] Moreover, there has been considerable debate as to whether the ATP level in the cell membrane is the same as that in cytosol.[22] Our results show that the cell membrane has the lower ATP concentrations.

The ATP level is regulated by cell metabolism and presents a dynamic equilibrium with oscillation characteristics on the order of minutes.[23] To test the response of DPTB-IMI-EG to the change of the ATP levels, apyrase was used to treat the cells prior to the co-staining procedure. Apyrase is an enzyme that catalyzes the hydrolysis of ATP to yield AMP and inorganic phosphate. When the cells were treated with 1 U mL^{-1} apyrase at 37 °C for 60 minutes, the fluorescence signals from DPTB-IMI-EG almost disappear, except for those close to the membrane (Figure 3 A2), thus suggesting a significant decrease in the ATP level in the cytoplasm. Meanwhile, MDRF still exhibits its specificity and sensitivity to the mitochondria (Figure 3 B2), thus further confirming no association between the indicator and the organelle. The low hydrolytic effect on membrane ATP levels may seem paradoxical by taking into account the fact that apyrase is exogenous. One possible explanation is that the enzyme associated with the microsomal fraction can show a significantly higher specific activity than the soluble one.[24] It is reasonable because apyrase can only be activated by calcium or magnesium, which is mainly distributed in microsome and endoplasmic reticulum.

Since the fluorescence lifetime is insensitive to several experimental parameters, such as excitation intensity, exposure duration, and photobleaching, the fluorescence lifetime imaging microscopy (FLIM) image may provide extra information compared to that from the intensity-based image. DPTB-IMI-EG exhibits dual fluorescence lifetimes originating from two different excited states of DPTB.[14] The average lifetime of the indicator shows a strong positive correlation with ATP levels (see Table S1). So the ATP spatial distribution was also examined with the FLIM technique. The ATP level obtained from FLIM is almost consistent with that from the fluorescence intensity method, though there are few differences in several bright granular regions (Figure 4). The intense fluorescence with short lifetime indicates that few organelles (probably the vacuole) can accumulate DPTB-IMI-EG through adsorption. Another piece of information provided by FLIM is the variation of the ATP levels during cell division. It can be seen from the intensity image (Figure 4 a) that the ATP distribution is broader in mitotic cells than in normal cells. The FLIM image demonstrates high intracellular ATP levels at the phase of mitosis, and is in

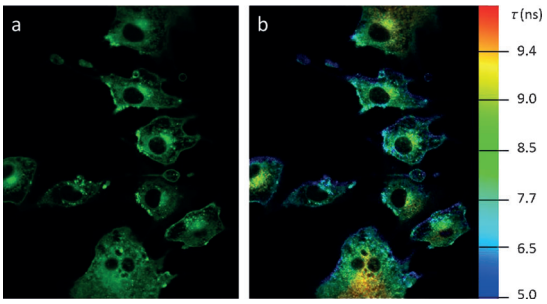

Figure 4. Confocal fluorescence images of live NIH/3T3 cells stained with DPTB-IMI-EG (1 μM) for 30 min in DMEM. a) Fluorescence intensity image. b) Merged intensity and lifetime image. Excitation wavelength: $\lambda = 405$ nm. Emission wavelength: $\lambda = 460$–550 nm.

compliance with the literature.[25] The above results reveal that DPTB-IMI-EG is a very good candidate for cell-cycle studies.

In conclusion, a novel triarylboron derivative with a hydrophilic, lipophilic, and amphiphilic three-block structure, has been synthesized and utilized as a fluorescent indicator for monitoring ATP levels in vitro and in vivo. It shows high specificity for ATP rather than ADP or AMP, and other bioactive species such as essential ions, amino acids, and several proteins show no apparent interference. The absorbance and luminescence are located in the visible region. The ATP-induced finite aggregation significantly enhances its photostability in the recognition process. The above advantages plus low cytotoxicity, good permeability and dispersibility, all suggest DPTB-IMI-EG to be a good imaging agent for ATP distribution and alteration tracking. The determinations of ATP levels in NIH/3T3 fibroblast cells have also been successfully performed with the indicator by using fluorescence microscopy and FLIM methods.

Received: April 2, 2014
Published online: June 6, 2014

Keywords: aggregation · cell recognition · fluorescence · imaging agents · molecular recognition

[1] a) J. R. Knowles, *Annu. Rev. Biochem.* **1980**, *49*, 877–919; b) R. Post, C. Merritt, C. R. Kinsolving, C. Albright, *J. Biol. Chem.* **1960**, *235*, 1796–1802; c) C. F. Higgins, I. D. Hiles, G. P. Salmond, D. R. Gill, J. A. Downie, I. J. Evans, I. B. Holland, L. Gray, S. D. Buckel, A. W. Bell, *Nature* **1986**, *323*, 448–450; d) R. Davies, *Nature* **1963**, *199*, 1068–1074.

[2] a) N. S. Mishra, R. Tuteja, N. Tuteja, *Arch. Biochem. Biophys.* **2006**, *452*, 55–68; b) M. Kamenetsky, S. Middelhaufe, E. M. Bank, L. R. Levin, J. Buck, C. Steegborn, *J. Mol. Biol.* **2006**, *362*, 623–639.

[3] M. P. Abbracchio, G. Burnstock, A. Verkhratsky, H. Zimmermann, *Trends Neurosci.* **2009**, *32*, 19–29.

[4] a) F. Özogul, K. D. A. Taylor, P. C. Quantick, Y. Özogul, *Int. J. Food Sci. Technol.* **2000**, *35*, 549–554; b) C. Fu, L. Song, Y. Fang, *Anal. Chim. Acta* **1999**, *399*, 259–263; c) D. A. Middleton, E. Hughes, M. Esmann, *Angew. Chem.* **2011**, *123*, 7179–7182; *Angew. Chem. Int. Ed.* **2011**, *50*, 7041–7044.

[5] J.-H. Kim, J.-H. Ahn, P. W. Barone, H. Jin, J. Zhang, D. A. Heller, M. S. Strano, *Angew. Chem.* **2010**, *122*, 1498–1501; *Angew. Chem. Int. Ed.* **2010**, *49*, 1456–1459.

[6] Y. Zhou, Z. Xu, J. Yoon, *Chem. Soc. Rev.* **2011**, *40*, 2222–2235.

[7] a) S. Nakano, M. Fukuda, T. Tamura, R. Sakaguchi, E. Nakata, T. Morii, *J. Am. Chem. Soc.* **2013**, *135*, 3465–3473; b) L.-M. Lu, X.-B. Zhang, R.-M. Kong, B. Yang, W. Tan, *J. Am. Chem. Soc.* **2011**, *133*, 11686–11691; c) J. Wang, L. Wang, X. Liu, Z. Liang, S. Song, W. Li, G. Li, C. Fan, *Adv. Mater.* **2007**, *19*, 3943–3946.

[8] a) G. V. Zyryanov, M. A. Palacios, P. Anzenbacher, *Angew. Chem.* **2007**, *119*, 7995–7998; *Angew. Chem. Int. Ed.* **2007**, *46*, 7849–7852; b) Z. Xu, N. J. Singh, J. Lim, J. Pan, H. N. Kim, S. Park, K. S. Kim, J. Yoon, *J. Am. Chem. Soc.* **2009**, *131*, 15528–15533; c) Y. Kurishita, T. Kohira, A. Ojida, I. Hamachi, *J. Am. Chem. Soc.* **2010**, *132*, 13290–13299.

[9] C. W. T. Leung, Y. Hong, S. Chen, E. Zhao, J. W. Y. Lam, B. Z. Tang, *J. Am. Chem. Soc.* **2013**, *135*, 62–65.

[10] H. Ow, D. R. Larson, M. Srivastava, B. A. Baird, W. W. Webb, U. Wiesner, *Nano Lett.* **2005**, *5*, 113–117.

[11] B.-K. An, S.-K. Kwon, S.-D. Jung, S. Y. Park, *J. Am. Chem. Soc.* **2002**, *124*, 14410–14415.

[12] Y. Hong, J. W. Y. Lam, B. Z. Tang, *Chem. Soc. Rev.* **2011**, *40*, 5361–5388.

[13] a) W. Z. Yuan, P. Lu, S. Chen, J. W. Y. Lam, Z. Wang, Y. Liu, H. S. Kwok, Y. Ma, B. Z. Tang, *Adv. Mater.* **2010**, *22*, 2159–2163; b) S.-J. Chung, K.-Y. Kwon, S.-W. Lee, J.-I. Jin, C. H. Lee, C. E. Lee, Y. Park, *Adv. Mater.* **1998**, *10*, 1112–1116; c) C. Zhang, Y. Yuan, S. Zhang, Y. Wang, Z. Liu, *Angew. Chem.* **2011**, *123*, 6983–6986; *Angew. Chem. Int. Ed.* **2011**, *50*, 6851–6854.

[14] J. Feng, K. Tian, D. Hu, S. Wang, S. Li, Y. Zeng, Y. Li, G. Yang, *Angew. Chem.* **2011**, *123*, 8222–8226; *Angew. Chem. Int. Ed.* **2011**, *50*, 8072–8076.

[15] B. Xiao, M. J. Sanders, E. Underwood, R. Heath, F. V. Mayer, D. Carmena, C. Jing, P. A. Walker, J. F. Eccleston, L. F. Haire, *Nature* **2011**, *472*, 230–233.

[16] a) M. M. T. Khan, A. E. Martell, *J.Phys. Chem.* **1962**, *66*, 10–15; b) R. S. Cooper, G. A. Altenberg, *J. Biol. Chem.* **2013**, *288*, 20785–20796.

[17] R. J. Ellis, *Trends Biochem. Sci.* **2001**, *26*, 597–604.

[18] S.-O. Ko, M. A. Schlautman, E. R. Carraway, *Environ. Sci. Technol.* **1998**, *32*, 3542–3548.

[19] D. S. Dos Santos, Jr., C. R. Mendonça, D. T. Balogh, A. Dhanabalan, A. Cavalli, L. Misoguti, J. A. Giacometti, S. C. Zilio, O. N. Oliveira, Jr., *Chem. Phys. Lett.* **2000**, *317*, 1–5.

[20] A. Ray, Y.-E. Koo Lee, T. Epstein, G. Kim, R. Kopelman, *Analyst* **2011**, *136*, 3616–3622.

[21] K. G. Hales, *Mitochondrion* **2004**, *4*, 285–308.

[22] F. M. Gribble, G. Loussouarn, S. J. Tucker, C. Zhao, C. G. Nichols, F. M. Ashcroft, *J. Biol. Chem.* **2000**, *275*, 30046–30049.

[23] V. C. Özalp, T. R. Pedersen, L. J. Nielsen, L. F. Olsen, *J. Biol. Chem.* **2010**, *285*, 37579–37588.

[24] M. A. Valenzuela, J. López, M. Depix, M. Mancilla, A. M. Kettlun, L. Catalán, M. Chiong, J. Garrido, A. Traverso-Cori, *Comp. Biochem. Physiol. Part B* **1989**, *93*, 911–919.

[25] Y. Yu, R. Dumollard, A. Rossbach, F. A. Lai, K. Swann, *J. Cell. Physiol.* **2010**, *224*, 672–680.

